Solvent Effects on Differentiation of Mouse Brain Tissue Using Laser Microdissection 'Cut and Drop' Sampling with Direct Mass Spectral Analysis

John F. Cahill[1]*, Vilmos Kertesz[1], Tiffany Porta[2], J. C. Yves LeBlanc[3], Ron M. A. Heeren[2], and Gary J. Van Berkel[1]

[1]Mass Spectrometry and Laser Spectroscopy Group, Chemical Sciences Division, Oak Ridge National Laboratory, Oak Ridge, TN 37831-6131, USA
[2]Maastricht MultiModal Molecular Imaging (M4I) institute, Division of Imaging Mass Spectrometry, Maastricht University, Universiteitssingel 50, 6229 ER Maastricht, The Netherlands
[3]Sciex, Concord, Ontario, Canada

*Corresponding Author:
John F. Cahill
Mass Spectrometry and Laser Spectroscopy Group
Chemical Sciences Division
Oak Ridge National Laboratory, Oak Ridge, TN 37831-6131
E-mail: cahilljf@ornl.gov
Phone: 865-574-4878

Running title: Mouse Brain Tissue Differentiation using Direct Mass Spectral Analysis

Keywords: Mass spectrometry, PCA, liquid capture, laser microdissection

Rapid Communications in Mass Spectrometry
DOI: 10.1002/rcm.8053

RATIONALE:

Laser microdissection-liquid vortex capture/electrospray ionization mass spectrometry (LMD-LVC/ESI-MS) has potential for on-line classification of tissue but an investigation into what analytical conditions provide best spectral differentiation has not been conducted. The effects of solvent, ionization polarity, and spectral acquisition parameters on differentiation of mouse brain tissue regions are described.

METHODS:

Individual 40 × 40 μm microdissections from cortex, white, grey, granular, and nucleus regions of mouse brain tissue were analyzed using different capture/ESI solvents, in positive and negative ion mode ESI, using time-of-flight (TOF)-MS and sequential window acquisitions of all theoretical spectra (SWATH)-MS (a permutation of tandem-MS), and combinations thereof. Principal component analysis-linear discriminant analysis (PCA-LDA), applied to each mass spectral dataset, was used to determine the accuracy of differentiation of mouse brain tissue regions.

RESULTS:

Mass spectral differences associated with capture/ESI solvent composition manifested as altered relative distributions of ions rather than the presence or absence of unique ions. In negative ion mode ESI, 80/20 (v/v) methanol/water yielded spectra with low signal/noise ratios relative to other solvents. PCA-LDA models acquired using 90/10 (v/v) methanol/chloroform differentiated tissue regions with 100% accuracy while data collected using methanol misclassified some samples. The combination of SWATH-MS and TOF-MS data improved differentiation accuracy.

CONCLUSIONS:

Combined TOF-MS and SWATH-MS data differentiated white, grey, granular, and nucleus mouse tissue regions with greater accuracy than when solely using TOF-MS data. Using 90/10 (v/v) methanol/ chloroform tissue regions were perfectly differentiated. These results will guide future studies looking to utilize the potential of LMD-LVC/ESI-MS for tissue and disease differentiation.

Introduction

Recent developments in ambient ionization mass spectrometry (MS) have enabled a wealth of new opportunities in the clinical environment.[1-3] For example, the ability of ambient ionization MS techniques to chemically characterize tissues rapidly and with minimal sample preparation has sparked interest towards using these technologies to guide surgical decisions in the operating room with greater throughput and confidence than is currently achievable.[1,2] While clinical applications utilizing ambient ionization MS techniques are still in their infancy, they have been increasingly used to explore biological tissue disease state identification and differentiation from normal 'healthy' tissue. In particular, desorption electrospray ionization (DESI) has been at the forefront of this movement over the last decade.[4-12] In most cases, emphasis has been placed on differentiating cancerous from healthy tissues. For instance, DESI mass spectral imaging has been used in combination with multivariate analyses to differentiate carcinomas in a variety of tissues, including prostate,[13-15] liver,[16,17] breast,[18,19] brain,[1,4,5,9,10,20] and others.[7,21-28] Several other ambient ionization MS techniques have similarly differentiated carcinomas from healthy tissue including probe-electrospray ionization (PESI)[29-31], rapid evaporative ionization MS (REIMS),[32,33] touch spray[13,14], laser desorption/ionization,[34,35] and others.[36-38] For ambient ionization MS techniques to be successful in the clinical environment, they must be highly sensitive, be able to differentiate tissue types with high spatial, spectral, and quantitative accuracy, and be easy to use.

Laser microdissection-liquid vortex capture electrospray ionization mass spectrometry (LMD-LVC/ESI-MS) is a recently developed ambient ionization MS technique that combines the capabilities of LMD, microscopy, and MS through the use of a liquid-vortex capture probe for sample collection and transport to the ESI source.[39-41] This technique has been shown to be highly sensitive relative to other ambient ionization MS techniques and it has enabled sub-micrometer spatial resolution MS imaging capabilities.[39] Unique to the system is the ability to perform 'cut and drop' (CnD) sampling in which whole tissue microdissections are cut and dropped using the laser from the microdissection system directly into the LVC probe.[40] This mode of sampling has several advantages, most notable of which is that it ensures 100% of sample material is captured into the LVC probe, a feature lacking in most

ambient ionization techniques. This feature makes it the most sensitive mode of operation for LMD-LVC/ESI-MS. The advantages of CnD sampling were demonstrated by quantifying propranolol present in hundreds of individual tissue microdissections from mouse brain, liver, and kidney tissue without any additional sample preparation or workup.[41] Further, since the LMD-LVC/ESI-MS technique couples two commercially available systems (i.e. LMD microscope and mass spectrometer) and does not require any modification of those systems beyond the addition of the LVC probe, there is potential for broad integration of the technique by utilizing existing laboratory infrastructure.

Outside the operating room, histopathology of formalin-fixed surgical biopsies is the standard method used for diagnosis of gliomas. Inside the operating room, histopathology of fresh frozen tissue biopsies is most commonly used to provide surgical guidance, as results can be obtained from a single biopsy in ~20 min.[2,42] However, the throughput of this process is low and diagnosis based solely on the pathologist can be susceptible to misclassification, most notably along the border of the carcinoma where differentiation of the disease state by optical microscopy becomes more ambiguous. The LMD-LVC/ESI-MS technique naturally synergizes with pathology-based approaches towards tissue diagnosis already used in the surgical environment, since a central component of the technique is optical microscopy. In addition to conventional diagnosis by a pathologist, CnD sampling/analysis by LMD-LVC/ESI-MS could be used to chemically characterize precise regional selections of tissue in an ‘on-line’ manner providing supplementary detail and improved confidence to diagnoses. In addition, the familiarity of LMD systems to clinicians and pathologists who routinely use optical microscopy for identification of tissue and the simplified integration with the mass spectrometer itself (i.e., no alignment needed between the LMD microscope and the mass spectrometer) make the LMD-LVC/ESI-MS system relatively easy to use. Hence, there is significant potential for integration of the LMD-LVC/ESI-MS technique into the clinical and surgical environment.

While LMD-LVC/ESI-MS has promise for applications in clinical settings, the ability of the technique to differentiate tissue types and the instrumental parameters that best serve to facilitate that differentiation have not been explored as of yet. To-date, on-line classification of several oils based on

atmospheric pressure chemical ionization mass spectra acquired using the open port sampling interface, a technique which is based on the same fundamental liquid extraction principals as LMD-LVC/ESI-MS, has been the only example of the differentiation capability of the technique.[43,44] In DESI, observed lipid profiles have been shown to be highly dependent on the solvent condition and ionization polarity used.[45,46] Mandal *et al*. investigated the effect of alcohol/water solvent mixtures on renal cell carcinoma lipid profiles measured using PESI and found that the addition of alcohol improved extraction of major lipids.[30] Likewise, Zhang *et al*. explored the effects of water/alcohol mixtures on lipid profiles and selected water for use due to its biocompatibility with living tissue.[36] While different lipid classes have been known to be observed between positive and negative ionization polarities, Jarmuch *et al*. recently showed that the combination of both ionization polarities with multivariate analysis improved the differentiation capabilities of DESI for distinguishing between normal and cancerous human brain tissue.[46]

In this work, the effect of the LMD-LVC/ESI-MS capture/ESI solvent composition, ionization polarity, and MS-scan conditions were investigated in terms of the ions observed, spectral signal/noise, and differentiation capability of mass spectra acquired using CnD sampling from small 40 × 40 µm microdissections of mouse brain tissue. Since the LMD-LVC/ESI-MS technique relies upon solvent to extract analytes from the dissected tissue during transport to the ionization source, solvent conditions are expected to have a major impact on the nature of mass spectra and the ability to differentiate between regions of tissue. Likewise, ESI polarity directly affects which classes of compounds are ionized and the overall informational content found in the mass spectra. Thus, the choice of ESI polarity may yield different degrees of differentiation capability. Lastly, the combination of several sequential window acquisitions of all theoretical spectra (SWATH)-MS[47] data in addition to time-of-flight (TOF)-MS data from the same tissue microdissection was investigated to determine whether the coupling of spectral acquisitions can improve the ability of the LMD-LVC/ESI-MS system to differentiate mouse brain tissue regions with high confidence. SWATH acquisitions are a permutation of tandem MS where ions in a wide *m/z* range are simultaneously fragmented via collision-induced dissociation. Thus, a single spectrum will collect TOF-MS data in a limited *m/z* range and product ion data for another *m/z* range. A valuable

advantage of SWATH in these experiments is the rapid simultaneous acquisition of product ion data during the narrow time widow available for analysis from a single microdissection (~1-2 s). The results reported here serve as the foundation for future studies using LMD-LVC/ESI-MS to differentiate diseased and healthy tissue.

Experimental

Chemicals and Materials

LC-MS CHROMASOLV® 100/0.1 (v/v) methanol/formic acid, methanol, ammonium acetate, chloroform, and water were purchased from Sigma-Aldrich (St. Louis, MO, USA). All animals used in this study were handled in accordance with the Guide for the Care and Use of Laboratory Animals[48] and provided by the Maastricht University Medical Center, Maastricht, The Netherlands (MUMC+). Mouse brain tissues were cryo-sectioned (Microtome cryostat; Thermo Scientific, Braunschweig, Germany) into 10-µm-thick tissue sections and subsequently thaw-mounted on 2.0 µm polyethylene naphthalate (PEN) membrane glass slides (#11505158; Leica Microsystems, Wetzel, Germany) and were stored at -80 °C prior to analysis by MS. Before analysis tissues were thawed at room temperature in a desiccator for 30 min.

LMD-LVC/ESI-MS

The LMD-LVC/ESI-MS system has been described in detail in previous publications.[39-41] Briefly, the system comprises a SCIEX Triple TOF® 5600+ mass spectrometer (Sciex, Concord, Ontario, Canada) coupled to a Leica LMD7000 system (Leica Microsystems) via a low-profile LVC probe. The UV laser (349 nm, 5 kHz maximum repetition rate, and 120 µJ maximum pulse energy) in the LMD7000 system was used for cutting whole tissue microdissections via the CnD sampling method.[40] This sampling method is fundamentally similar to the laser pressure "catapulting"[49,50] technique described in LMD literature except that the tissue microdissections are captured into the solvent of the LVC probe rather than a capture cap. Once in the solvent, analytes are extracted from the tissue and dissolved during

transport to the ionization source of the mass spectrometer. The concept for laser CnD sampling for tissues is illustrated in Figure 1(A). First, the outline of a square shaped 20 × 20, 40 × 40, or 80 × 80 µm area of tissue is laser ablated, creating an independent tissue microdissection. The microdissection remains suspended on the sample slide by static forces and adhesion to the glass substrate. A short laser pulse aimed at the center of the microdissection ejects it away from the glass backing and gravity brings the microdissection down towards the LVC probe where it is captured into the solvent. The solvent extracts analytes from the microdissection while transporting it to the ionization source of the mass spectrometer. Specific LMD laser settings used in the LMD7000 software (version 7.5.1) for cutting and ejecting tissue microdissections were power = 30, attenuation = 10, head current = 100, and pulse frequency = 5000 Hz with the 20X objective.

The LVC probe consists of a co-axial tube arrangement with a 1.12/1.62 mm (i.d./o.d.) outer stainless-steel probe and a 0.178/0.794 mm (i.d./o.d.) inner PEEK capillary. The probe was located 1 mm below the sample surface. Detrimental airflows near the probe were minimized by covering the LMD7000 with a plastic sheet and by attaching a sheath made of heat shrink tubing to the LVC probe that extended 1.1 mm above the top of the probe (~0.1 mm from the sample surface). The solvent flow rate was optimized to achieve a stable liquid vortex for each solvent and ionization condition. Flow rates used for each solvent condition are provided in Table S1 (Supporting Information).

The mass spectrometer was configured to acquire TOF mass spectra (mass/charge (*m/z*) 600-1000) along with SWATH-MS scans.[47] Three different SWATH-MS acquisition scan windows were used in this study: SWATH-1 = *m/z* 700-775, SWATH-2 = *m/z* 775-850, and SWATH-3 = *m/z* 850-925. A rolling collision energy from 20-50 eV with a *m/z* 100-1000 product ion window was set for each SWATH acquisition. A 0.25 s scan time, 100 V declustering potential, 300 °C turbo heater temperature, and GS1 = 90 and GS2 = 60 N_2 nebulizer gas settings were held constant across all experiments.

Principal Component Analysis-Linear Discriminant Analysis (PCA-LDA)

PCA-LDA analysis was conducted using MATLAB® (Mathworks, Natick, MA, USA). Spectra

were normalized and binned into 0.01 *m/z* segments resulting in 40,000 data points per TOF mass spectrum and 90,000 points for every SWATH® spectrum. Spectra were mass corrected based on a series of identified ions from known molecules present in each spectrum. A 'combined' spectrum comprised of appended TOF, SWATH-1, SWATH-2, and SWATH-3 mass spectra (310,000 points) was used to investigate if SWATH acquisitions would improve model accuracies. A subset of data for each solvent condition tested was reserved for determination of optimal PCA-LDA spectral inputs and component selection. Cross-validation of each model permutation was calculated using the 'leave-one-out' cross-validation method. For simplicity and practicality, only combinations of the top 5 principal components were explored for model generation. Once the optimal PCA-LDA model was selected, the remaining test data was used to determine the model apportionment accuracy for 100/0.1 (v/v) methanol/formic acid, 90/10 (v/v) methanol/chloroform, 100% methanol + 10mM ammonium acetate, and 90/10 (v/v) methanol/chloroform + 10mM ammonium acetate solvent conditions.

Results

Effects of capture solvent and ESI polarity on ions observed in TOF and SWATH spectral acquisitions

LVC capture solvent and ESI polarity are hypothesized to greatly affect the number and classes of ions present in mass spectra which in turn will affect the differentiating capabilities of the LMD-LVC/ESI-MS system. Cortex, white matter, grey matter, granular matter, and nucleus mouse brain tissue regions were identified by a pathologist using adjacent H&E stained tissue sections (Figure 1(B)). Small 40 × 40 µm microdissections were sampled from each tissue region (Figure 1(A)) using CnD sampling with 80/20/0.1 (v/v/v) methanol/water/formic acid, 100/0.1 (v/v) methanol/formic acid, or 90/10 (v/v) methanol/chloroform as the capture/ESI solvent. Average TOF mass spectra for each tissue region and solvent condition are shown in Figure 2. Given the small volume of the tissue microdissections ($1.6 \cdot 10^{-5}$ mm^3), the signal/noise ratio (S/N) of mass spectra was rather high especially when using 100/0.1 (v/v) methanol/formic acid (maximum S/N = 188, 223, and 1429 for cortex tissue using 80/20/0.1 (v/v/v)

methanol/water/formic acid, 90/10 (v/v) methanol/chloroform, or 100/0.1 (v/v) methanol/formic acid, respectively). The relative distributions of characteristic ions in TOF-MS spectra from cortex tissue were virtually identical across microdissections 20 × 20, 40 × 40, and 80 × 80 μm in size sampled while using 90/10 (v/v) methanol/chloroform (Figure S1, Supporting Information). Assuming that the lipids present in this tissue type are homogeneously distributed, this data demonstrates that little material needs to be sampled to obtain characteristic markers. This finding was true for all tissue types and solvent conditions investigated.

The ions in the positive ion mass spectra correspond primarily to the protonated molecules, $[M + H]^+$ ions, of glycerophosphochloline (PC) and glycerophosphoethanolamine (PE) lipids between *m/z* 700 and 900. A list of identified lipids and ions (>10% relative intensity) for each tissue region and solvent condition is provided in Table S2 (Supporting Information). Identifications were based on observed *m/z* values, SWATH acquisitions, separate tandem-MS experiments (data not shown), and literature publications.[29,51-55] For example, PC lipids were identified based on the characteristic product ion in tandem-MS experiments at *m/z* 184 corresponding to the choline headgroup $[C_5H_{14}NPO_4 + H]^+$ and PE lipids were identified by the neutral loss of the ethanolaminephosphate headgroup (loss of 141 Da).[54-56] The major observable lipids were PC(32:0)/PE(35:0), PC(34:1)/PE(37:1), PC(34:0)/PE(37:0), PC(36:1), PC(38:6), PC(38:4), and PC(40:6) with $[M + H]^+$ ions at *m/z* 734.54, 760.55, 762.56, 788.58, 806.53, 810.64, and 834.56, respectively. In the few cases having both PC and PE identifications, e.g., *m/z* 734.54 (PC(32:0)/PE(35:0)), product ions indicating the presence of both lipids were observed using tandem-MS. It is likely that the PC lipid was present at a much higher relative concentration than the PE lipid based on the intensity of the choline headgroup product ion in these situations, and this may also explain why they were not fully resolved in the TOF-MS spectra. PC(32:0)/PE(35:0) and PC(34:0)/PE(37:0) were greater in intensity in cortex, granular, and grey matter tissue types while PC(36:1) was present in greater intensity in nucleus and white matter tissue. PC(40:6) was located primarily in granular and grey matter tissue types. A number of ions having *m/z*

between 800.61-851.64 (e.g., PC(38:4) and PC(40:6) at *m/z* 810.64 and 834.56, respectively) were enhanced when sampling from white matter using 100/0.1 (v/v) methanol/formic acid and 90/10 (v/v) methanol/chloroform solvents as compared to 80/20/0.1 (v/v/v) methanol/water/formic acid . A similar trend was observed for nucleus tissue, but only when using 90/10 (v/v) methanol/chloroform. Combined SWATH spectra, acquired simultaneously with TOF-MS spectra (Figure S2, Supporting Information), were dominated by the choline headgroup, *m/z* 184.12, for every tissue region and solvent condition.[52-55] Most other product ions observed in SWATH data, e.g., *m/z* 630.71, can be attributed to the neutral loss of the ethanolaminephosphate headgroup. Overall when using positive ion mode ESI, spectral heterogeneity between tissue regions and capture/ESI solvents was mainly caused by changes in the relative ratio of the major lipid ions present in all the spectra rather than the arrival of completely unique signatures.

Negative ion mode ESI-MS mass spectra, in contrast to positive ion mode, had a more diverse array of lipid species and exhibited greater spectral heterogeneity between tissue regions and solvent conditions. TOF-MS spectra for different solvent conditions and tissue regions collected in negative ion ESI mode are shown in Figure 3 and their identifications are given in Table S3 (Supporting Information). Spectra obtained for cortex tissue when using 80/20 (v/v) methanol/water + 10 mM ammonium acetate exhibited notably weaker spectra (maximum S/N = 36) than when using 90/10 (v/v) methanol/chloroform + 10 mM ammonium acetate or 100% methanol + 10 mM ammonium acetate (maximum S/N = 130 and 160, respectively). Ions present at *m/z* 768.53 (PE(38:3)), 792.56 (PC(16:0)/(16:0)), 818.56 (PC(16:0)/(18:1)), 834.52 (PS(40:6)), 846.61 (PS(40:0)), 862.64 (ST(22:0)), and 885.53 (PI(38:4)) were identified as a combination of PE, PC, glycerophosphoserines (PS), glycerophosphoinositols (PI), and sulfatide (ST) lipids based upon SWATH spectra (Figure S3, Supporting Information), previous literature reports,[46,51,55,57,58] and separate tandem-MS data (data not shown). These lipids were observed in their deprotonated form, $[M - H]^-$, though notable exceptions to this were the acetate (Ac) adducts $[M + Ac]^-$ of the PC lipids, (PC(16:0)/(16:0) and PC(16:0)/(18:1), at *m/z* 792.56 and 818.56, respectively. The product ions observed in SWATH spectra were

predominantly fatty acid (FA) anions, e.g., *m/z* 255.23 (FA(16:0)), 281.25 (FA(18:1)), 303.23 (FA(20:4)), and 327.23 (FA(22:6)). The spectra obtained with 100% methanol + 10 mM ammonium acetate were largely similar to those with 90/10 (v/v) methanol/chloroform + 10 mM ammonium acetate with a few notable exceptions, especially evident when comparing grey matter tissue. The acetate adducts of PC lipids at *m/z* 792.56 (PC(16:0)/(16:0)) and 818.56 (PC(16:0)/(18:1)) dominated the mass spectrum of grey matter when using 100% methanol + 10 mM ammonium acetate, while *m/z* 834.52 (PS(40:6)) and 885.53 (PI(38:4)) were much greater in relative intensity when using 90/10 (v/v) methanol/chloroform + 10 mM ammonium acetate. The SWATH spectra were similar across all solvent conditions and tissue regions, differing mostly in relative intensity. In TOF-MS data, grey matter could be spectrally differentiated from white matter and nucleus tissue regions by ions *m/z* 834.52 (PS(40:6)) and 885.53 (PI(38:4)) present in grey matter and ions *m/z* 888.60, 890.62, and 906.63 corresponding to ST(24:1), ST(24:0), and ST(h24:0), respectively, present in white matter and nucleus tissue. These differences have also been observed in other studies.[29,46] Granular matter and cortex tissue had spectral features present in white matter, grey matter, and nucleus tissue types.

PCA-LDA Differentiation of Tissue Types

One of the objectives of this work was to determine which solvent condition, ionization polarity, spectral acquisition method, and combinations thereof, facilitate the best statistical differentiation of mouse brain tissue regions. Spectra acquired with the LMD-LVC/ESI-MS system using 90/10 (v/v) methanol/chloroform, 100/0.1 (v/v) methanol/formic acid, 90/10 (v/v) methanol/chloroform + 10 mM ammonium acetate, and 100% methanol + 10 mM ammonium acetate were selected for investigation of their spectral differentiation capabilities by PCA-LDA. The data obtained using 80/20 (v/v) methanol/water had significantly weaker signals in the negative ion mode and had very few if any uniquely identifying peaks and thus was not tested for PCA-LDA classification. A total of 61 microdissections, 40 × 40 μm in size, taken from four different tissue regions, viz., white matter, grey matter, granular, and nucleus tissue regions (15-16 samples in each region), were analyzed using 90/10 (v/v)

methanol/chloroform, 100/0.1 (v/v) methanol/formic acid, 90/10 (v/v) methanol/chloroform + 10 mM ammonium acetate, and 100% methanol + 10 mM ammonium acetate resulting in a total of 244 microdissections measured. For each solvent tested, the data was split into training and test datasets (comprising 30 and 31 randomly selected microdissections, respectively). The training data was used to compare the accuracies of identification between each spectral acquisition type, while the test dataset was used to compare accuracies of identification between capture/ESI-solvents using the acquisition type identified with the training data.

The leave-one-out cross-validation of the PCA-LDA accuracies for PCA models using the top 2 and 3 principal components of the training dataset is summarized in Table 1. PCA-LDA models were created using TOF-MS and combined TOF-MS and SWATH-MS spectra. Other combinations utilizing permutations of the top 5 principal components were explored, but resulted in similar to or worse accuracies than those presented in Table 1 (data not shown). For every solvent condition the combined TOF-MS and SWATH-MS spectra had equal to or greater accuracy than when solely using TOF-MS data. Most notably, the combination of TOF-MS and SWATH-MS improved accuracies when using 100/0.1 (v/v) methanol/formic acid and 100% methanol + 10 mM ammonium acetate by 13% relative to when using only TOF-MS data. In addition, the identification accuracies for PCA-LDA models using the top 3 principal components were near 100% for every solvent condition when using both TOF-MS and SWATH-MS data. Based on these findings, combined TOF-MS and SWATH-MS data was used for subsequent analysis.

PCA-LDA models can be constructed using any permutation of any number of available principal components. For comparison of capture/ESI solvent effects on tissue region classification, only the first three principal components were used herein for the following reasons. First, the variance in mass spectra captured by each individual principal component beyond the third was <5%. A plot showing the steep drop-off in percentage spectral variance captured by each principal component beyond the third is shown for each solvent condition using combined TOF-MS and SWATH-MS data in Figure S4 (Supporting Information). Secondly, leave-one-out cross-validation of all PCA-LDA model

permutations using the first 5 principal components resulted in the same accuracy of identification as when using the first 3 principal components. Thus, based on developing the simplest model with best accuracy only the top 3 components are needed. Lastly, leave-one-out cross-validation accuracies using the first 3 principal components resulted in near perfect accuracies for each solvent condition suggesting that the inclusion of additional components would be superfluous.

The resulting PCA-LDA models made using the training dataset for each solvent condition are shown in Figure 4. Three-dimensional (3D) moving visualizations of each PCA-LDA model in Figure 4 are provided in Movies S1-4 (Supporting Information). The accuracies of each PCA-LDA model and the total variance covered by the model are summarized in Table 2. All the models fared well with only three misidentified tissue components out of 124 total validation samples. The incorrectly classified points were when using 100/0.1 (v/v) methanol/formic acid (1 incorrectly identified) and 100% methanol + 10 mM ammonium acetate (2 incorrectly identified) solvent conditions. Both 90/10 (v/v) methanol/chloroform and 90/10 (v/v) methanol/chloroform + 10 mM ammonium acetate PCA-LDA models were able to identify tissue regions from the test dataset without any misclassifications. To further verify the model, an additional 62 microdissections (15-16 areas sampled from each tissue region) were acquired using 90/10 (v/v) methanol/chloroform in positive ion mode and were classified without error. Thus, these results indicate that 90/10 (v/v) methanol/ chloroform in positive or negative ion mode should be used in future studies.

Conclusion

We have demonstrated the capability of the LMD-LVC/ESI-MS system for the differentiation of white, grey, granular, and nucleus mouse brain tissue matter using PCA-LDA of small 40 × 40 µm tissue microdissections. Hundreds of individual microdissections were analyzed on-line without clogging or maintenance of the LVC probe being required. While there was spectral heterogeneity between tissue regions, in general, mass spectral differences between solvent conditions for a given ESI polarity and

tissue region were mostly evident by changes to the relative distribution of ions rather than the arrival of completely unique features. Of the solvent and ionization conditions explored, 80/20 (v/v) methanol/water fared the worst, yielding spectra containing only a few uniquely identifying ions that were of lower S/N than those from other solvent compositions. In comparison, 90/10 (v/v) chloroform/methanol and 100% methanol in either positive or negative ion ESI mode yielded TOF-MS and SWATH-MS spectra with greater intensity and more discriminating spectral features.

The combination of TOF-MS and SWATH-MS acquisitions improved accuracies of PCA-LDA model tissue region identification compared with when using solely TOF-MS data. Since TOF-MS and SWATH-MS acquisitions can both be collected from the same signal transient of an individual tissue microdissection (1-2 s), there is little reason not to implement both acquisitions in future studies. While SWATH spectra were dominated by PC headgroup ions in the positive ion mode, the identification of simultaneously measured PS, PE, PC, and PI product ions in the negative ion mode serves as an example of the differentiating power that SWATH mass spectra can provide in addition to TOF-MS. PCA-LDA cross-validation results indicated that a 3-component PDA-LDA model using combined TOF and SWATH mass spectra would most accurately classify the different tissue regions sampled. A PCA-LDA model made using 90/10 (v/v) methanol/chloroform in either positive or negative ESI mode was best able to classify tissue regions, with no incorrect classifications of 31 and 93 test samples, respectively. In comparison, methanol solvent conditions in positive and negative ion mode resulted in 1 and 2 misclassifications, respectively, out of 31 test samples. Thus, in future studies of brain tissue it is recommended that the 90/10 (v/v) methanol/chloroform solvent system be used to facilitate classification.

Acknowledgements

The original advancement of the LMD-LVC/ESI-MS system was supported at ORNL by the U. S. Department of Energy, Office of Science, Basic Energy Sciences, Chemical Sciences, Geosciences, and

Biosciences Division. T. Porta and R.M.A. Heeren acknowledge support of the LINK program of the Dutch Province of Limburg. We are grateful to Audrey Jongen (General Surgery, MUMC+) for providing us with the mouse brain sample and Lieke Lamont (M4I) for her technical assistance. The present application of the technology was supported at ORNL by, and the SCIEX TripleTOF® 5600+ mass spectrometer used in this work was provided on loan through, a Cooperative Research and Development Agreement with Sciex (CRADA NFE-10-02966). Julian Burke (Leica Microsystems) is thanked for the loan of the LMD7000 instrument.

References

1. Calligaris D, Norton I, Feldman DR, et al. Mass spectrometry imaging as a tool for surgical decision-making. *J Mass Spectrom.* 2013;48(11):1178-1187.

2. Ifa DR, Eberlin LS. Ambient ionization mass spectrometry for cancer diagnosis and surgical margin evaluation. *Clin Chem.* 2016;62(1):111-123.

3. Takats Z, Strittmatter N, Mckenzie JS. Chapter nine - Ambient mass spectrometry in cancer research. In: Drake RR, ed. *Advances in Cancer Research*. London, UK: Academic Press; 2017.

4. Calligaris D, Feldman DR, Norton I, et al. Molecular typing of meningiomas by desorption electrospray ionization mass spectrometry imaging for surgical decision-making. *Int J Mass Spectrom.* 2015;377:690-698.

5. Eberlin LS, Norton I, Orringer D, et al. Ambient mass spectrometry for the intraoperative molecular diagnosis of human brain tumors. *Proc Natl Acad Sci.* 2013;110(5):1611-1616.

6. Eberlin LS, Margulis K, Planell-Mendez I, et al. Pancreatic cancer surgical resection margins: Molecular assessment by mass spectrometry imaging. *PLOS Med.* 2016;13(8):e1002108.

7. Eberlin LS, Tibshirani RJ, Zhang J, et al. Molecular assessment of surgical-resection margins of gastric cancer by mass-spectrometric imaging. *Proc Natl Acad Sci.* 2014;111(7):2436-2441.

8. Agar NYR, Golby AJ, Ligon KL, et al. Development of stereotactic mass spectrometry for brain tumor surgery. *Neurosurgery.* 2011;68(2):280-290.

9. Eberlin LS, Norton I, Dill AL, et al. Classifying human brain tumors by lipid imaging with mass spectrometry. *Cancer Res.* 2012;72(3):645-654.

10. Santagata S, Eberlin LS, Norton I, et al. Intraoperative mass spectrometry mapping of an onco-metabolite to guide brain tumor surgery. *Proc Natl Acad Sci.* 2014;111(30):11121-11126.

11. Jarmusch AK, Pirro V, Baird Z, Hattab EM, Cohen-Gadol AA, Cooks RG. Lipid and metabolite profiles of human brain tumors by desorption electrospray ionization-ms. *Proc Natl Acad Sci.* 2016;113(6):1486-1491.

12. Pirro V, Alfaro CM, Jarmusch AK, Hattab EM, Cohen-Gadol AA, Cooks RG. Intraoperative assessment of tumor margins during glioma resection by desorption electrospray ionization-mass spectrometry. *Proc Natl Acad Sci.* 2017;114(26):6700-6705.

13. Kerian KS, Jarmusch AK, Cooks RG. Touch spray mass spectrometry for in situ analysis of complex samples. *Analyst.* 2014;139(11):2714-2720.

14. Kerian KS, Jarmusch AK, Pirro V, et al. Differentiation of prostate cancer from normal tissue in radical prostatectomy specimens by desorption electrospray ionization and touch spray ionization mass spectrometry. *Analyst.* 2015;140(4):1090-1098.

15. Eberlin LS, Dill AL, Costa AB, et al. Cholesterol sulfate imaging in human prostate cancer tissue by desorption electrospray ionization mass spectrometry. *Anal Chem.* 2010;82(9):3430-3434.

16. Wiseman JM, Puolitaival SM, Takats Z, Cooks RG, Caprioli RM. Mass spectrometric profiling of intact biological tissue by using desorption electrospray ionization. *Angew Chem Int Ed Engl.* 2005;44(43):7094-7097.

17. Dill AL, Ifa DR, Manicke NE, Ouyang Z, Cooks RG. Mass spectrometric imaging of lipids using desorption electrospray ionization. *J Chromatogr B Analyt Technol Biomed Life Sci.* 2009;877(26):2883-2889.

18. Calligaris D, Caragacianu D, Liu X, et al. Application of desorption electrospray ionization mass spectrometry imaging in breast cancer margin analysis. *Proc Natl Acad Sci.* 2014;111(42):15184-15189.

19. Guenther S, Muirhead LJ, Speller AV, et al. Spatially resolved metabolic phenotyping of breast cancer by desorption electrospray ionization mass spectrometry. *Cancer Res.* 2015;75(9):1828-1837.

20. Eberlin LS, Dill AL, Golby AJ, et al. Discrimination of human astrocytoma subtypes by lipid analysis using desorption electrospray ionization imaging mass spectrometry. *Angew Chem Int Ed Engl.* 2010;49(34):5953-5956.

21. Masterson TA, Dill AL, Eberlin LS, et al. Distinctive glycerophospholipid profiles of human seminoma and adjacent normal tissues by desorption electrospray ionization imaging mass spectrometry. *J Am Soc Mass Spectrom.* 2011;22(8):1326-1333.

22. Dill AL, Eberlin LS, Zheng C, et al. Multivariate statistical differentiation of renal cell carcinomas based on lipidomic analysis by ambient ionization imaging mass spectrometry. *Anal Bioanal Chem.* 2010;398(7-8):2969-2978.

23. Dill AL, Eberlin LS, Costa AB, et al. Multivariate statistical identification of human bladder carcinomas using ambient ionization imaging mass spectrometry. *Chemistry.* 2011;17(10):2897-2902.

24. Eberlin LS, Gabay M, Fan AC, et al. Alteration of the lipid profile in lymphomas induced by

MYC overexpression. *Proc Natl Acad Sci*. 2014;111(29):10450-10455.

25. Gerbig S, Golf O, Balog J, et al. Analysis of colorectal adenocarcinoma tissue by desorption electrospray ionization mass spectrometric imaging. *Anal Bioanal Chem.* 2012;403(8):2315-2325.

26. Abbassi-Ghadi N, Veselkov K, Kumar S, et al. Discrimination of lymph node metastases using desorption electrospray ionisation-mass spectrometry imaging. *Chem Commun.* 2014;50(28):3661-3664.

27. Woolman M, Tata A, Dara D, et al. Rapid determination of the tumour stroma ratio in squamous cell carcinomas with desorption electrospray ionization mass spectrometry (DESI-MS): A proof-of-concept demonstration. *Analyst.* 2017;142(17):3250-3260.

28. D'hue C, Moore M, Summerlin D-J, et al. Feasibility of desorption electrospray ionization mass spectrometry for diagnosis of oral tongue squamous cell carcinoma. *Rapid Commun Mass Spectrom*. 2017. https://doi.org/10.1002/rcm.8019.

29. Otsuka Y, Naito J, Satoh S, Kyogaku M, Hashimoto H, Arakawa R. Imaging mass spectrometry of a mouse brain by tapping-mode scanning probe electrospray ionization. *Analyst.* 2014;139(10):2336-2341.

30. Mandal MK, Yoshimura K, Chen LC, et al. Application of probe electrospray ionization mass spectrometry (PESI-MS) to clinical diagnosis: Solvent effect on lipid analysis. *J Am Soc Mass Spectrom.* 2012;23(11):2043-2047.

31. Mandal MK, Saha S, Yoshimura K, et al. Biomolecular analysis and cancer diagnostics by negative mode probe electrospray ionization. *Analyst.* 2013;138(6):1682-1688.

32. Balog J, Sasi-Szabó L, Kinross J, et al. Intraoperative tissue identification using rapid evaporative

ionization mass spectrometry. *Sci Transl Med.* 2013;5(194):194ra193.

33. Golf O, Strittmatter N, Karancsi T, et al. Rapid evaporative ionization mass spectrometry imaging platform for direct mapping from bulk tissue and bacterial growth media. *Anal Chem.* 2015;87(5):2527-2534.

34. Fatou B, Saudemont P, Leblanc E, et al. In vivo real-time mass spectrometry for guided surgery application. *Sci Rep.* 2016;6,25919. doi: 10.1038/srep25919.

35. Schäfer K-C, Szaniszló T, Günther S, et al. In situ, real-time identification of biological tissues by ultraviolet and infrared laser desorption ionization mass spectrometry. *Anal Chem.* 2011;83(5):1632-1640.

36. Zhang J, Rector J, Lin JQ, et al. Nondestructive tissue analysis for ex vivo and in vivo cancer diagnosis using a handheld mass spectrometry system. *Sci Transl Med.* 2017;9(406):eaan3968.

37. Schafer KC, Balog J, Szaniszlo T, et al. Real time analysis of brain tissue by direct combination of ultrasonic surgical aspiration and sonic spray mass spectrometry. *Anal Chem.* 2011;83(20):7729-7735.

38. Mandal MK, Yoshimura K, Saha S, et al. Solid probe assisted nanoelectrospray ionization mass spectrometry for biological tissue diagnostics. *Analyst.* 2012;137(20):4658-4661.

39. Cahill JF, Kertesz V, Van Berkel GJ. Characterization and application of a hybrid optical microscopy/laser ablation liquid vortex capture/electrospray ionization system for mass spectrometry imaging with sub-micrometer spatial resolution. *Anal Chem.* 2015;87(21):11113-11121.

40. Cahill JF, Kertesz V, Van Berkel GJ. Laser dissection sampling modes for direct mass spectral analysis. *Rapid Commun Mass Spectrom.* 2016;30(5):611-619.

41. Cahill JF, Kertesz V, Weiskittel TM, Vavrek M, Freddo C, Van Berkel GJ. Online, absolute quantitation of propranolol from spatially distinct 20- and 40-µm dissections of brain, liver, and kidney thin tissue sections by laser microdissection-liquid vortex capture-mass spectrometry. *Anal Chem.* 2016;88(11):6026-6034.

42. Novis DA, Zarbo RJ. Interinstitutional comparison of frozen section turnaround time. A college of american pathologists q-probes study of 32868 frozen sections in 700 hospitals. *Arch Pathol Lab Med.* 1997;121(6):559-567.

43. Van Berkel GJ, Kertesz V. An open port sampling interface for liquid introduction atmospheric pressure ionization mass spectrometry. *Rapid Commun Mass Spectrom.* 2015;29(19):1749-1756.

44. Van Berkel GJ, Kertesz V. Rapid sample classification using an open port sampling interface coupled with liquid introduction atmospheric pressure ionization mass spectrometry. *Rapid Commun Mass Spectrom.* 2017;31(3):281-291.

45. Badu-Tawiah AK, Eberlin LS, Ouyang Z, Cooks RG. Chemical aspects of the extractive methods of ambient ionization mass spectrometry. *Annu Rev Phys Chem.* 2013;64:481-505.

46. Jarmusch AK, Alfaro CM, Pirro V, Hattab EM, Cohen-Gadol AA, Cooks RG. Differential lipid profiles of normal human brain matter and gliomas by positive and negative mode desorption electrospray ionization - mass spectrometry imaging. *PLoS One.* 2016;11(9):e0163180.

47. Gillet LC, Navarro P, Tate S, et al. Targeted data extraction of the MS/MS spectra generated by data-independent acquisition: A new concept for consistent and accurate proteome analysis. *Mol. Cell Proteomics.* 2012;11(6):O111.016717.

48. National Research Council (US) Committee for the Update of the Guide for the Care and Use of Laboratory Animals. *Guide for the Care and Use of Laboratory Animals*. 8th ed. Washington,

DC: National Academy Press (US); 2011.

49. Schutze K, Lahr G. Identification of expressed genes by laser-mediated manipulation of single cells. *Nat Biotechnol.* 1998;16(8):737-742.

50. Schutze K, Posl H, Lahr G. Laser micromanipulation systems as universal tools in cellular and molecular biology and in medicine. *Cell Mol Biol.* 1998;44(5):735-746.

51. Eberlin LS, Ferreira CR, Dill AL, Ifa DR, Cooks RG. Desorption electrospray ionization mass spectrometry for lipid characterization and biological tissue imaging. *Biochim Biophys Acta.* 2011;1811(11):946-960.

52. Nemes P, Woods AS, Vertes A. Simultaneous imaging of small metabolites and lipids in rat brain tissues at atmospheric pressure by laser ablation electrospray ionization mass spectrometry. *Anal Chem.* 2010;82(3):982-988.

53. Almeida R, Berzina Z, Arnspang EC, et al. Quantitative spatial analysis of the mouse brain lipidome by pressurized liquid extraction surface analysis. *Anal Chem.* 2015;87(3):1749-1756.

54. Brügger B, Erben G, Sandhoff R, Wieland FT, Lehmann WD. Quantitative analysis of biological membrane lipids at the low picomole level by nano-electrospray ionization tandem mass spectrometry. *Proc Natl Acad Sci.* 1997;94(6):2339-2344.

55. Han X. *Lipidomics: comprehensive mass spectrometry of lipids*. Hoboken, NJ: John Wiley & Sons, Inc; 2016.

56. Xia YQ, Jemal M. Phospholipids in liquid chromatography/mass spectrometry bioanalysis: Comparison of three tandem mass spectrometric techniques for monitoring plasma phospholipids, the effect of mobile phase composition on phospholipids elution and the association of phospholipids with matrix effects. *Rapid Commun Mass Spectrom.* 2009;23(14):2125-2138.

57. Carson RH, Lewis CR, Erickson MN, et al. Imaging regiospecific lipid turnover in mouse brain with desorption electrospray ionization mass spectrometry. *J Lipid Res.* 2017;58(9):1884-1892.

58. Moe MK, Anderssen T, Strom MB, Jensen E. Total structure characterization of unsaturated acidic phospholipids provided by vicinal di-hydroxylation of fatty acid double bonds and negative electrospray ionization mass spectrometry. *J Am Soc Mass Spectrom.* 2005;16(1):46-59.

Table Captions:

Table 1: PCA-LDA model accuracy determined using leave-one-out cross-validation of the training dataset (30 samples for each solvent) when using the top 2 and top 3 principal components.

Table 2: PCA-LDA model accuracy using the top 3 principal components and combined TOF-MS and SWATH-MS spectra acquired for each solvent condition. Training samples were used to generate the PCA-LDA model while test samples were used for model validation.

Figure Captions:

Figure 1: (A) Cartoon of the laser 'cut and drop' sampling procedure. (B) Selected regions of mouse brain tissue under investigation in this study.

Figure 2: Positive ion mode ESI-TOF mass spectra from 40 × 40 μm tissue sections acquired from the different tissue regions and solvent conditions indicated in the figure. Major ions are annotated and identification of the ions by tandem MS are compiled in Table S2 (Supporting Information).

Figure 3: Negative ion mode ESI-TOF mass spectra from 40 × 40 μm tissue sections acquired from the different tissue regions and solvent conditions indicated in the figure. Major ions are annotated and identification of the ions by tandem MS are compiled in Table S3 (Supporting Information).

Figure 4: Three component PCA models of combined TOF and SWATH mass spectra for (A) 90/10 (v/v) methanol/chloroform positive ion mode ESI, (B) 90/10 (v/v) methanol/chloroform + 10 mM ammonium acetate negative ion mode ESI, (C) 100/0.1 (v/v) methanol/formic acid positive ion mode ESI, and (D) 100% methanol + 10 mM ammonium acetate negative mode ESI. Open circles represent the training samples used to generate the PCA-LDA model. Filled circles and asterisks represent correctly and incorrectly classified test samples, respectively.

Solvent	Components 1+2		Components 1+2+3	
	TOF-MS	Combined TOF+SWATH-MS	TOF-MS	Combined TOF+SWATH-MS
90/10 (v/v) methanol/chloroform	97%	97%	97%	97%
90/10 (v/v) methanol/chloroform + 10 mM ammonium acetate	83%	97%	90%	97%
100/0.1 (v/v) methanol/formic acid	87%	100%	87%	100%
100% methanol + 10 mM ammonium acetate	80%	93%	87%	100%

Table 1: PCA-LDA model accuracy determined using leave-one-out cross-validation of the training dataset (30 samples for each solvent) using the top 2 and top 3 principal components.

Solvent	Accuracy (%)	Training Samples	Test Samples
90/10 (v/v) methanol/chloroform	100%	30	31+62
90/10 (v/v) methanol/chloroform + 10 mM ammonium acetate	100%	30	31
100/0.1 (v/v) methanol/formic acid	97%	30	31
100% methanol + 10 mM ammonium acetate	94%	30	31

Table 2: PCA-LDA model accuracy using the top 3 principal components and combined TOF-MS and SWATH-MS spectra acquired for each solvent condition. Training samples were used to generate the PCA-LDA model while test samples were used for model validation.

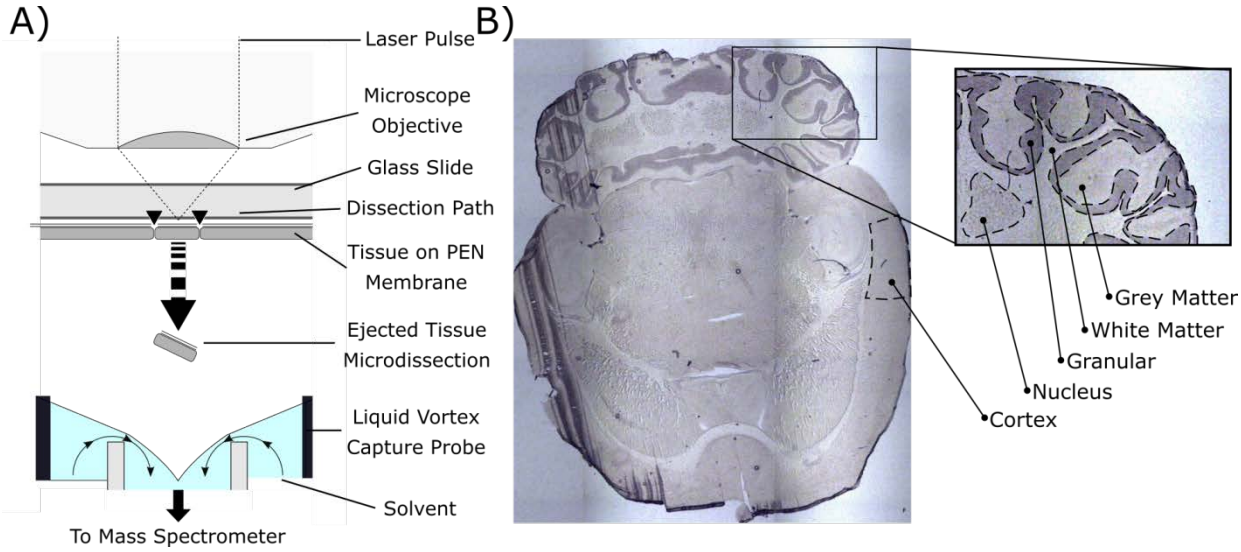

Figure 1: (A) Cartoon of the laser 'cut and drop' sampling procedure. (B) Selected regions of mouse brain tissue under investigation in this study.

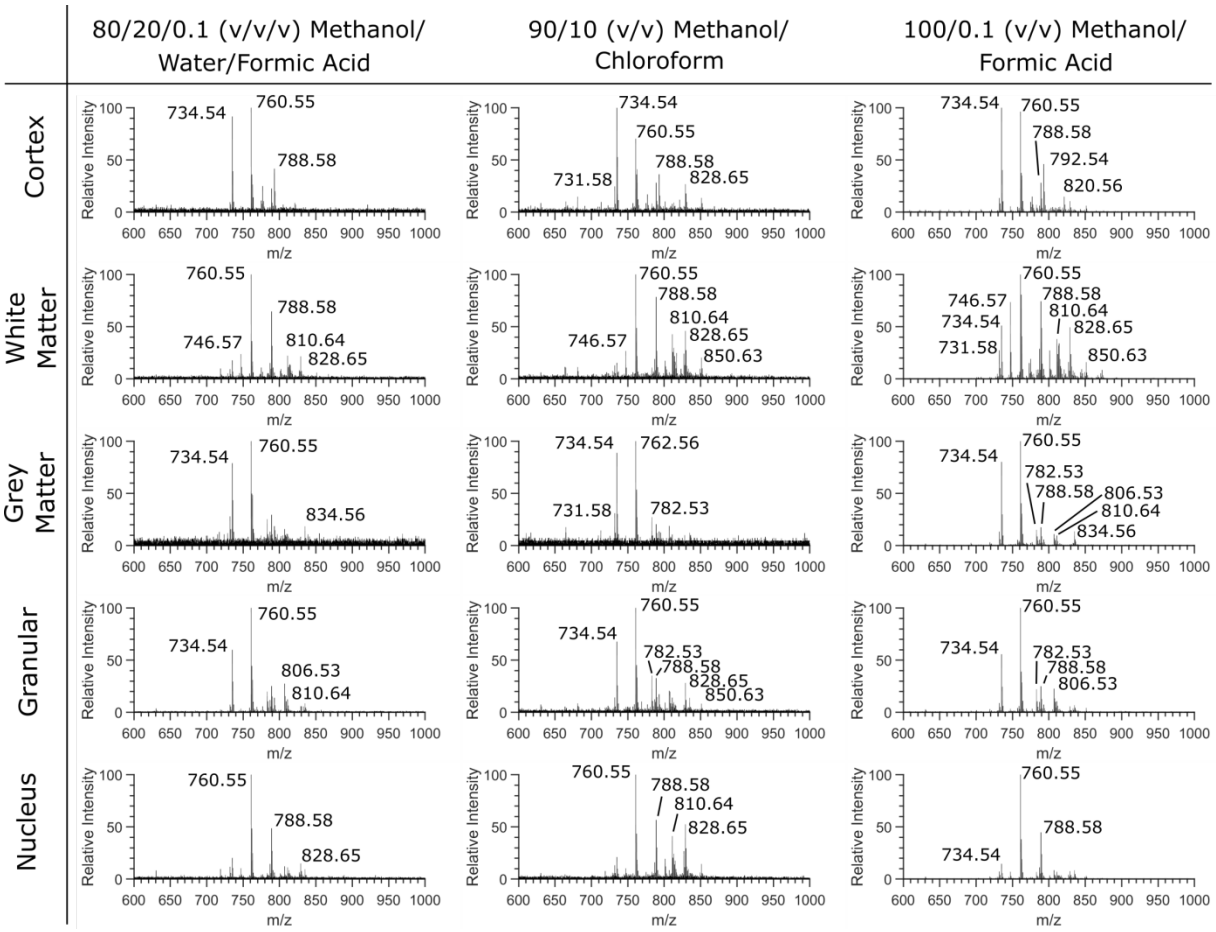

Figure 2: Positive ion mode ESI-TOF mass spectra from 40 × 40 µm tissue sections acquired from the different tissue regions and solvent conditions indicated in the figure. Major ions are annotated and identification of the ions by tandem MS are compiled in Table S2 (Supporting Information).

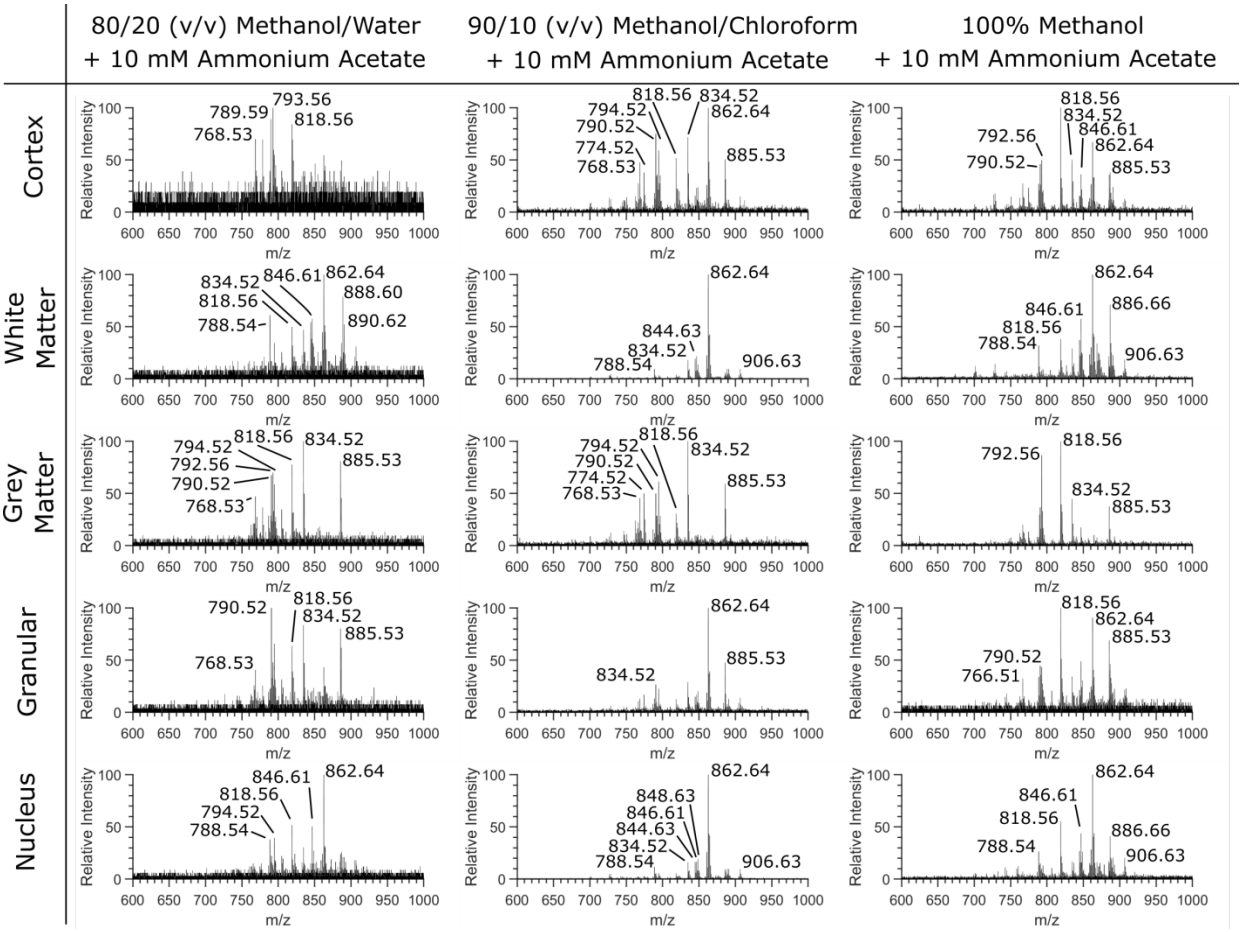

Figure 3: Negative ion mode ESI-TOF mass spectra from 40 × 40 µm tissue sections acquired from the different tissue regions and solvent conditions indicated in the figure. Major ions are annotated and identification of the ions by tandem MS are compiled in Table S3 (Supporting Information).

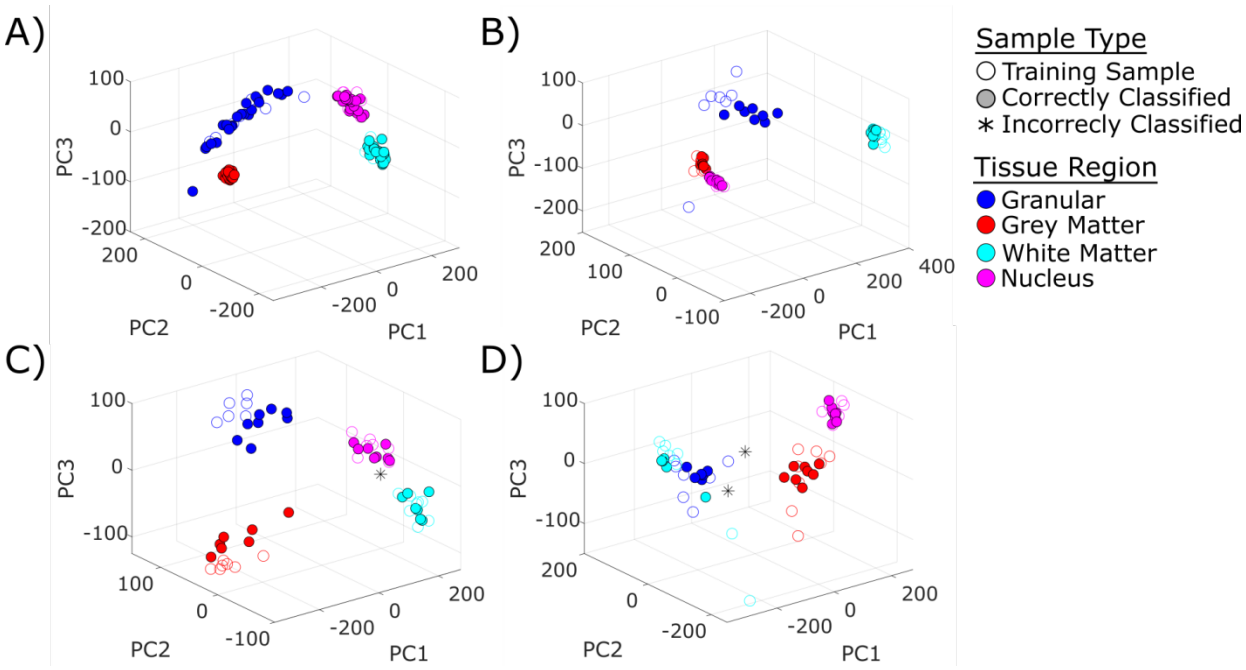

Figure 4: Three component PCA models of combined TOF and SWATH mass spectra for (A) 90/10 (v/v) methanol/chloroform positive ion mode ESI, (B) 90/10 (v/v) methanol/chloroform + 10 mM ammonium acetate negative ion mode ESI, (C) 100/0.1 (v/v) methanol/formic acid positive ion mode ESI, and (D) 100% methanol + 10 mM ammonium acetate negative mode ESI. Open circles represent the training samples used to generate the PCA-LDA model. Filled circles and asterisks represent correctly and incorrectly classified test samples, respectively.